Supporting Information

April 4, 2024

Contents

1 Model Parameters

These parameters for the organic components were taken from the OPLS force field[1] and the charges were generated using LigParGen[2] and the 1.14*CM1A utility[3]. The parameters for the surfaces were taken from the CLAYFF force field with Kerisit corrections for Fe.[4–7]

Atom type	ϵ kcal mol^{-1}	σ Å	Charge
alkyl C	0.066	3.500	-
alkyl H	0.030	2.500	-
aromatic C	0.070	3.550	-
aromatic H	0.030	2.420	-
O in OH	0.170	3.120	-
H in OH	0.000	0.000	-
ether O	0.140	2.900	-
amine N	0.170	3.300	-
amine H	0.000	0.000	-
Fe (Tetrahedral)	9.0263 $\times 10^{-6}$	4.072	+1.575
Fe (Octahedral)	9.0263 $\times 10^{-6}$	4.072	+1.3125
O in surface	0.1554	3.165541	-1.050
O in OH in surface	0.1554	3.165541	-0.950
H in OH in surface	0.000	0.00	+0.425

Table S1: Parameters used in the simulation

1.0.1 DGEBA

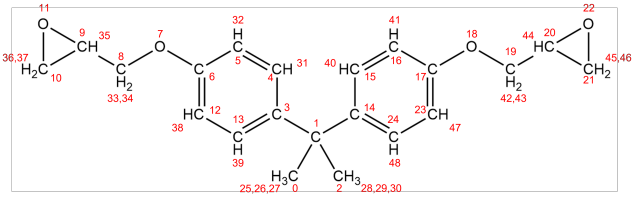

Figure S1: Structure of DGEBA with atom indices labelled in red.

Table S2: OPLS-AA atom properties of DGEBA.[1]

Atom Index	Atom Type	Charge q / e
0	CT	-0.2304
1	CT	0.0462
2	CT	-0.2304
3	CA	-0.1046
4	CA	-0.0944
5	CA	-0.1974
6	CA	0.1226
7	OS	-0.2962
8	CT	0.0071
9	CT	-0.0499
10	CT	-0.0787
11	OS	-0.3343
12	CA	-0.1974
13	CA	-0.0944
14	CA	-0.1046
15	CA	-0.0944
16	CA	-0.1974
17	CA	0.1226
18	OS	-0.2962
19	CT	0.0071
20	CT	-0.0499
21	CT	-0.0787
22	OS	-0.3343
23	CA	-0.1974
24	CA	-0.0944

Atom Index	Atom Type	Charge q / e
25	HC	0.0882
26	HC	0.0882
27	HC	0.0882
28	HC	0.0882
29	HC	0.0882
30	HC	0.0882
31	HA	0.1462
32	HA	0.1504
33	HC	0.11
34	HC	0.11
35	HC	0.1635
36	HC	0.1418
37	HC	0.1418
38	HA	0.1504
39	HA	0.1462
40	HA	0.1462
41	HA	0.1504
42	HC	0.11
43	HC	0.11
44	HC	0.1635
45	HC	0.1418
46	HC	0.1418
47	HA	0.1504
48	HA	0.1462

1.0.2 MXDA

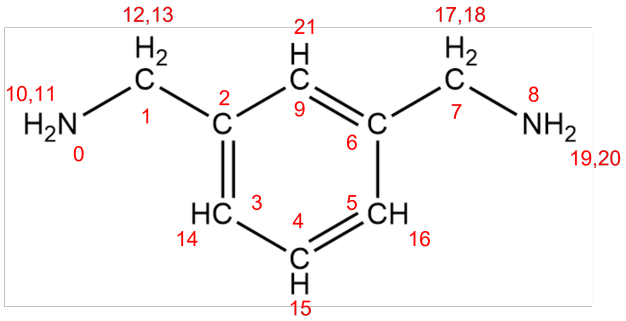

Figure S2: Structure of MXDA with atom indices labelled in red.

Table S3: OPLS-AA atom properties of MXDA.[1]

Atom Index	Atom Type	Charge q / e
0	NT	-0.90755
1	CT	0.12655
2	CA	-0.1007
3	CA	-0.1155
4	CA	-0.1472
5	CA	-0.1155
6	CA	-0.1007
7	CT	0.12655
8	NT	-0.90755
9	CA	-0.1015
10	HN2	0.33185
11	HN2	0.33185
12	HC	0.08545
13	HC	0.08545
14	HA	0.1423
15	HA	0.1401
16	HA	0.1423
17	HC	0.08545
18	HC	0.08545
19	HN2	0.33185
20	HN2	0.33185
21	HA	0.1492

2 Simulation details

Where a range of temperatures is specified, the temperature is linearly interpolated over the simulation time.

Table S4: Temperature and ensemble details of the first step of film preparation, prior to inserting the surface.

Ensemble	Temperature / K	Time / ps
NVT	0.1 - 1000	50
NVT	1000	400
NVT	1000 - 500	500
NVT	500	100
NPT	500	500

Table S5: Temperature and ensemble details of an annealing cycle from the second step of film preparation, prior to inserting the surface. This annealing cycle is repeated 5 times

Ensemble	Temperature / K	Time / ps
NVT	500	200
NVT	500 - 1000	200
NVT	1000	1000
NVT	1000 - 500	500

Table S6: Temperature and ensemble details of the simulation once the surface has been inserted underneath the film.

Ensemble	Temperature / K	Time / ps
NVT	500 - 295/323/393	500
NVT	295/323/393	1000

3 NP$_z$T Pressure Equilibration

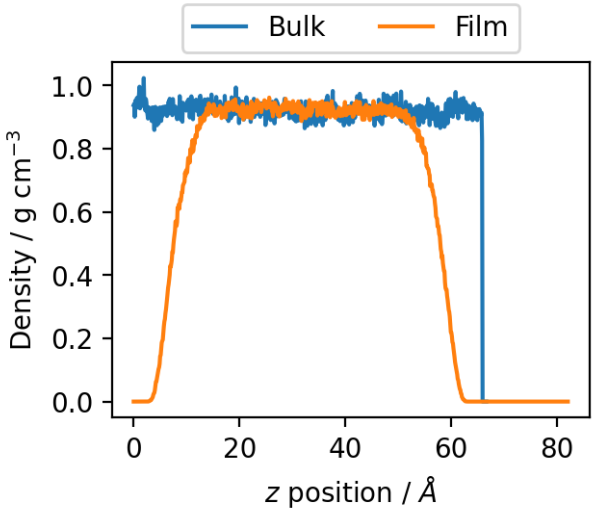

Figure S3: Bulk and harmonic wall induced film density plots of a 400 DGEBA, 200 MXDA system at 500 K, showing the same average density in the bulk regions of both.

4 Annealing Simulation Results

To ensure complete mixing of the DGEBA-MXDA mixture prior to the introduction of a surface, radial distribution functions (RDFs) were calculated from each of the 200 ps 500 K steps of the annealing cycle (Table S5), averaged over snapshots taken each 1 ps. The mixture is expected to be fully mixed when the RDF shows no significant change between annealing cycles. For each surface used, example RDFs are shown at each annealing step in Figure S5. Note that since at this stage the surface has not yet been introduced, the only difference between the films is the box dimensions, but an example of each is included for completeness.

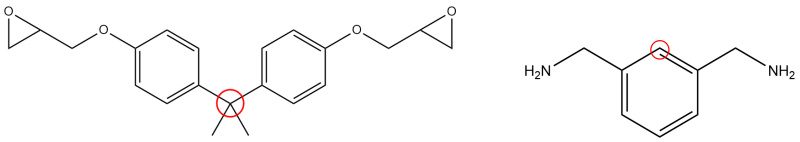

(a) (b)

Figure S4: Skeletal structures of DGEBA and MXDA, with central carbon atoms used for calculating RDFs indicated with red circles.

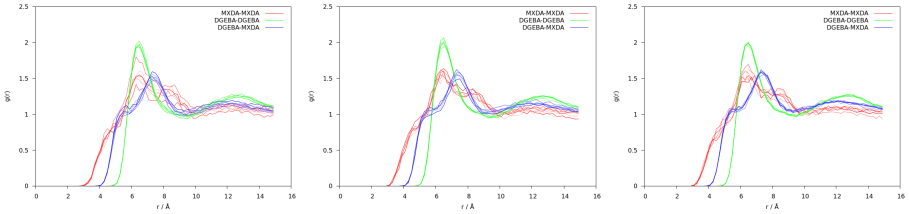

(a) (b) (c)

Figure S5: RDFs of DGEBA-MXDA film mixtures during each 200 ps, 500 K step of the annealing cycle prior to surface introduction. For each surface (a) hematite, (b) magnetite and (c) goethite, one example film is used, with RDFs shown in lower saturation for early annealing cycles and more saturated for later cycles. DGEBA-DGEBA RDFs are shown in green, MXDA-MXDA RDFs shown in red and DGEBA-MXDA RDFs shown in blue. The central reference atoms used to calculate the RDFs are shown in Figure S4.

5 Surface Structures

The structures of each iron oxide surface used in this work are shown below. From this, the presence of topmost iron atoms in hematite and topmost hydroxyl groups in goethite can be seen, while magnetite has both iron and oxide atoms in the topmost layer of atoms. Figure S6a shows the hexagonal pattern of iron atoms in the topmost plane of hematite, which results in an hexagonal arrangement of pockets due to the stacking of the layers below. Figure S6d shows the diagonal arrangement of iron atoms in magnetite, and each iron atom surrounded by four oxygen atoms in the topmost plane. The pockets in magnetite result from the lower oxygen atoms between rows of octahedral iron atoms, and Figure S6g shows the square arrangement of iron and oxygen atoms in goethite with pockets between iron atoms and hydroxyl oxygen atoms.

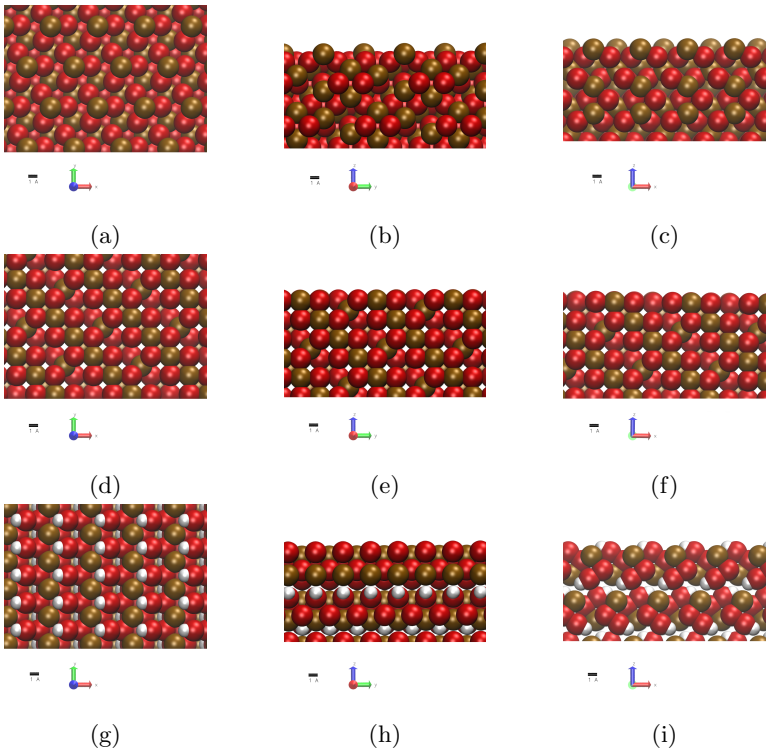

Figure S6: Surface structure renders of (a,b,c) hematite, (d,e,f) magnetite, and (g,h,i) goethite, shown in the (a,d,g) xy plane, (b,e,h) yz plane and (c,f,i) zx plane. Iron atoms are shown in ochre, oxygen atoms in red and hydrogen atoms in white. A 1 Å scale bar is shown by each render, as well as an indication of the axes.

6 Magnetite Artefact

When using a single slab of Magnetite(100), simulation artefacts are observed in the monomer phase, shown in Figure S7. This artefact was removed by inserting an additional slab underneath the simulation box, rotated by 180°along the x axis (Figure S8). Therefore, it is expected that this artefact is a result of long-range electrostatic dipole interactions, which are eliminated by inclusion of this second flipped and opposite dipolar surface.

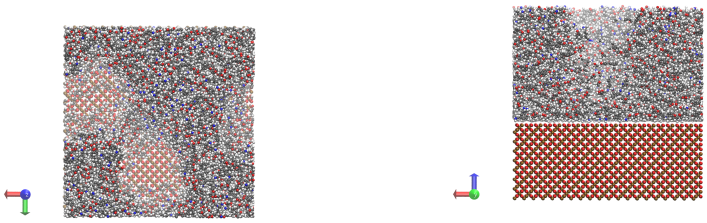

(a) (b)

Figure S7: Magnetite/monomer system with a single magnetite(100) surface, resulting in unphysical polymer dewetting of the surface in patches, shown (a) parallel and (b) perpendicular to the surface. Carbon atoms are shown as grey spheres, oxygen as red spheres, hydrogen as white spheres, nitrogen as blue spheres and iron as ochre spheres.

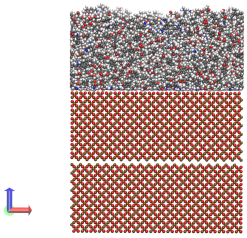

Figure S8: Magnetite/monomer system using an additional, flipped magnetite(100) surface to eliminate the net dipole moment of the system and remove simulation artefacts.

Since performing the simulations in this work, the authors have become aware of the slab correction to the PPPM model[8] available in LAMMPS using the *kspace_modify slab* function. This is able to remedy the artefacts observed here, without the additional system size and computational cost of the system used in this work. To verify that the results are unaffected by the differences in simulation setup, the linear concentration profiles for the magnetite with an

additional inverted slab and for the magnetite with the slab correction are shown below, with negligible differences between the two.

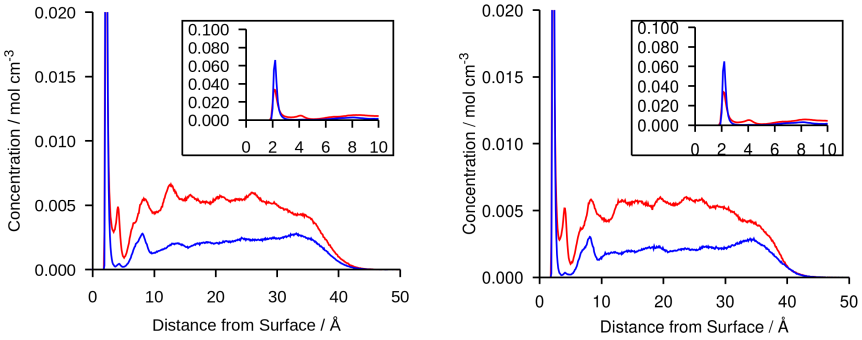

Figure S9: Linear concentration profiles of DGEBA epoxide oxygen (red) and MXDA nitrogen (blue) atoms with respect to distance from a magnetite surface. Systems are simulated using (a) full 3D PPPM long-range electrostatic corrections, and (b) 2D PPPM long-range electrostatic corrections using the slab method proposed by Yeh *et al.*[8] Both plots are averaged over 5 independent simulations.

7 Surface-Adsorbed Film Linear Density

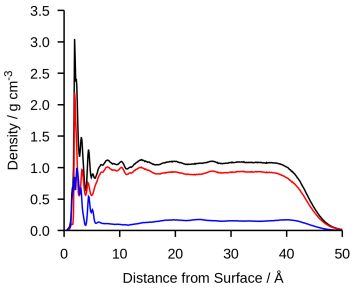

(a)

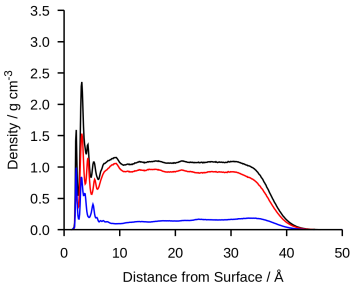

(b)

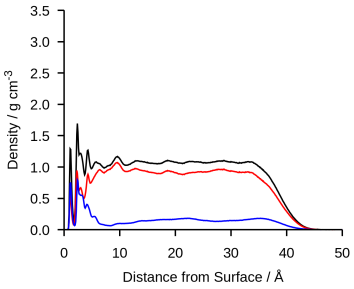

(c)

Figure S10: Linear density plots of a 400 DGEBA, 200 MXDA film at 323 K averaged over the last 1 ns of 5 independent simulations when adsorbed to (a) hematite, (b) magnetite and (c) goethite. In each plot, the total density is shown in black, DGEBA partial density is shown in red and MXDA partial density is shown in blue. Density is used here to show the distribution of mass of the whole film, whereas concentration is used in Figure 4 to directly compare the presence of epoxy oxygen and nitrogen atoms.

8 Segregation Equilibration

The validity of the 1 ns period used for averaging adsorbate quantities is verified by performing a simulation with a 2 ns constant final temperature NVT section. Averages are taken over the whole 2 ns, as well as over the first 1 ns interval. This is performed for one representative 400 DGEBA, 200 MXDA, hematite system at 323 K. The resulting linear concentration plots are shown in Figure S11. Only slight fluctuations are seen in the noise in the bulk film region, with negligible change to the first adsorption peak. Therefore, the 1 ns averaging period is determined to be sufficient to capture an equilibrated system.

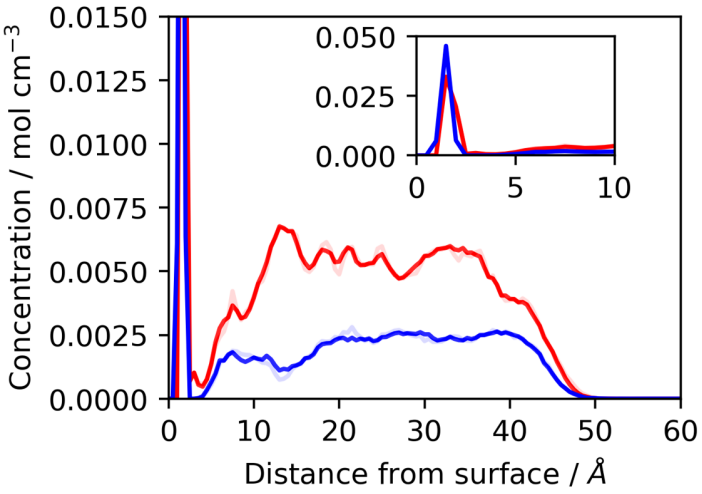

Figure S11: Linear concentration plot of epoxy oxygen (red) and amine nitrogen (blue) atoms as a function of distance from a hematite surface in a single simulation. High saturation plots indicate an average over 2 ns of 323 K simulation, while low saturation plots indicate an average over just the first 1 ns of the same simulation.

9 Large Surface Simulation

A single stoichiometric DGEBA/MXDA simulation was performed using a goethite surface expanded by a factor of 2 in the x and y dimensions. 1600 DGEBA and 800 MXDA molecules were included in the film to maintain the same thickness. Linear concentration plots of the average 8×8 nm^2 goethite simulations and the 16×16 nm^2 goethite simulation are shown respectively in Figure S12. The mean N:O ratio in 8×8 nm surface simulations was 1.35, with a standard deviation of 0.24, and the N:O ratio in the 16×16 nm surface simulation was 1.33, showing a negligible difference.

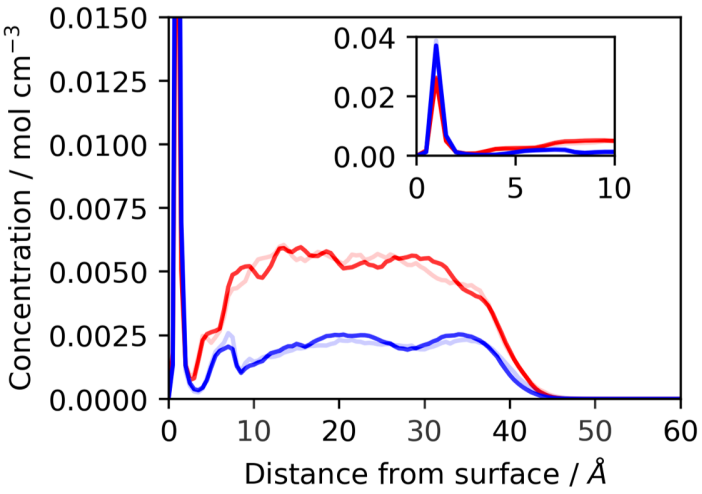

Figure S12: Linear concentration plots of epoxy oxygen (red) and amine nitrogen (blue) atoms as a function of distance from a goethite surface. High saturation plots indicate the approximately 8×8 nm^2 surface system, while low saturation plots indicate the 16×16 nm^2 surface system.

10 Temperature Dependence

Figure S13 shows no significant effect of temperature on the average surface monomer ratios relative to the effects of the structure of the surfaces.

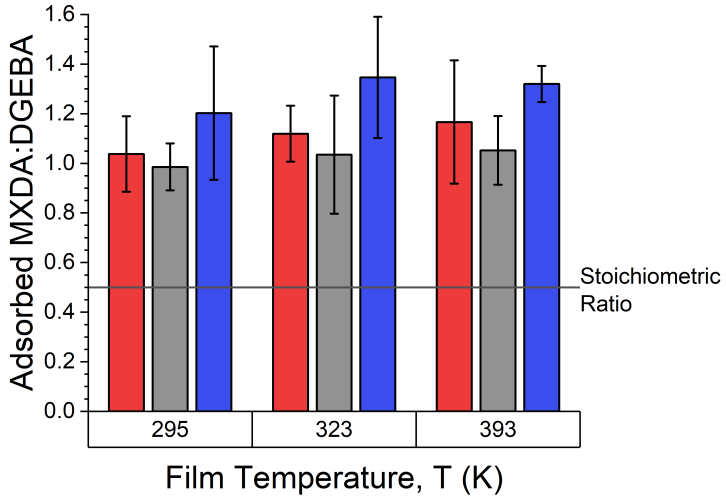

Figure S13: Surface-adsorbed monomer ratios at different temperatures. Surface type is indicated by bar colour, with red corresponding to hematite, grey to magnetite and blue to goethite. The stoichiometric MXDA:DGEBA ratio of 0.5 is indicated by a solid grey line.

11 Adsorption Isotherm

11.1 Fitting Function

In this simple model, the assumption is made that the adsorbed and bulk phases are at equilibrium and that all possible adsorption sites are occupied. Given the system is binary, the mole fractions of components i and j in bulk (x_i) and adsorbed (y_i) are related by the following respective equations,

$$x_i + x_j = 1 \tag{1}$$

$$y_i + y_j = 1. \tag{2}$$

Assuming the fugacity of a component in a given phase is proportional to its mole fraction and that the adsorbed mole fraction y_i is proportional to the bulk fugacity, we can write that

$$y_i = a_i x_i. \tag{3}$$

Given Equations 2 and 3,

$$y_i = \frac{a_i x_i}{a_j x_j + a_i x_i}. \tag{4}$$

If we define the partition coefficient as $k_i = a_i/a_j$,

$$y_i = \frac{k_i x_i}{x_j + k_i x_i} \tag{5}$$

and finally, using Equation 1, we can obtain an equation for the mole fraction of the adsorbed phase:

$$y_i = \frac{k_i x_i}{1 + (k_i - 1)x_i}. \tag{6}$$

11.2 Film Compositions

The compositions of films used to investigate the surface behaviour at varied DGEBA:MXDA ratios is shown below. The amounts of each monomer were chosen to keep the total number of atoms close to 24000, the number of atoms in the 400 DGEBA : 200 MXDA film. This keeps the total film volume approximately constant, since MXDA is a significantly smaller molecule than DGEBA.

Table S7: Compositions of films used to determine the surface-induced segregation behaviour of DGEBA:MXDA mixtures at varied composition ratios.

% DGEBA	% MXDA	# DGEBA	# MXDA	# Atoms
0	100	0	1090	23980
20	80	170	700	23730
40	60	290	430	23670
60	40	370	250	23630
66	33	400	200	24000
80	20	440	110	23980
100	0	480	0	23520

The regions defined in order to calculate amounts of DGEBA and MXDA in the surface-adsorbed and bulk regions are depicted on the example linear number density plots below.

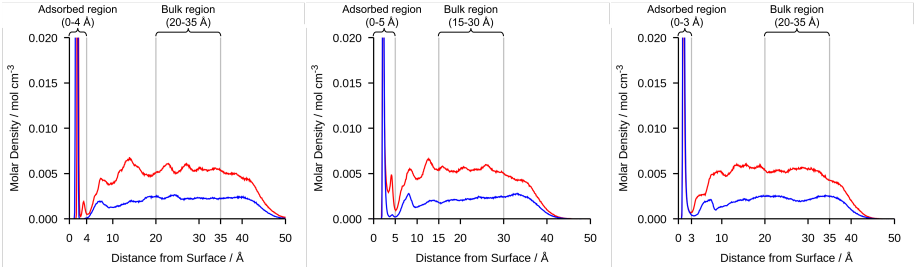

(a) (b) (c)

Figure S14: Definitions of bulk and surface-adsorbed regions shown on linear number density plots of a 400 DGEBA, 200 MXDA film for (a) hematite, (b) magnetite and (c) goethite.

12 Monomer Bulk Intramolecular Distances

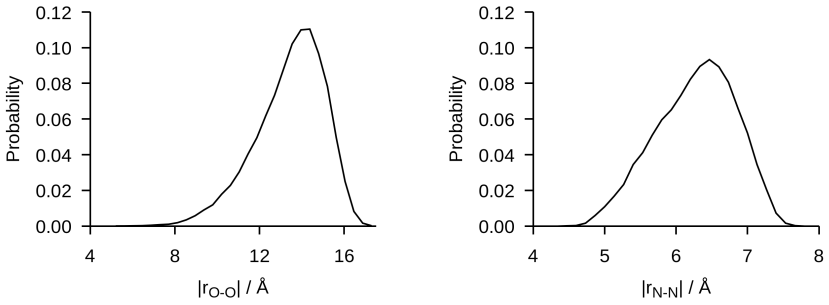

(a) (b)

Figure S15: Bulk intramolecular heteroatom distance distribution of (a) DGEBA and (b) MXDA at 323 K.

13 Binding Mode Heat Maps

Below, the binding mode heat maps are shown for DGEBA and MXDA with the inclusion of partially-bound molecules (i.e. only one epoxy or amine group bound to the surface). In the case of MXDA, in which only 25% of molecules are partially bound, there is an additional faint adsorption mode at values of $r_{aro-surface}$ of 5 Å for hematite and goethite, and 6 Å for magnetite. However, the longer and more flexible DGEBA is able to span a much wider range of values of $r_{CT-surface}$ when partially bound, resulting in a significantly noisier heat map. This makes it difficult to discern the presence of different binding modes, so their contribution was removed from the heat maps used in the main paper.

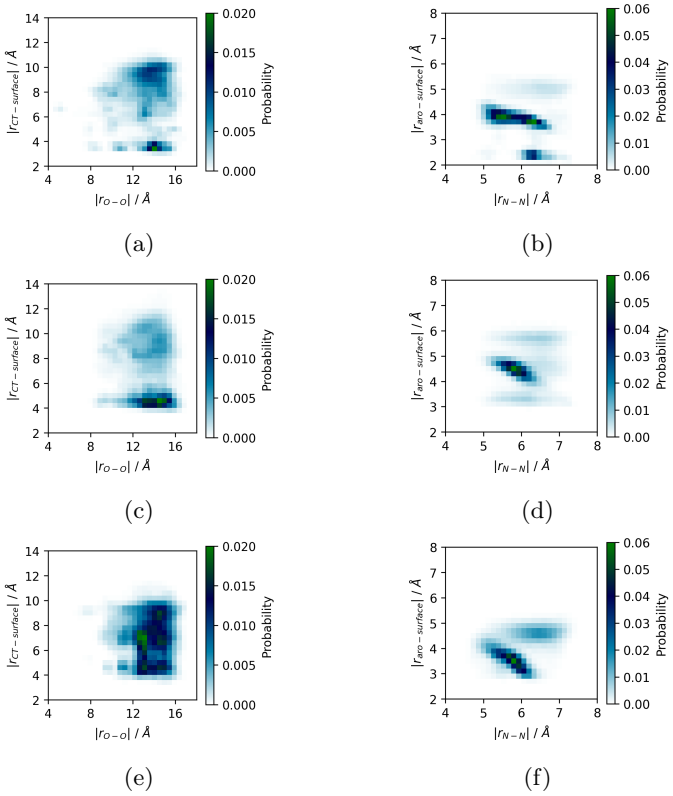

Figure S16: Histograms of binding mode probability at (a,b) hematite, (c,d) magnetite and (e,f) goethite surfaces, shown for (a,c,e) DGEBA and (b,d,f) MXDA. These are equivalent to those shown in the main paper, but include part-bound molecule contributions.

References

[1] Jorgensen, W. L.; Tirado-Rives, J. Potential energy functions for atomic-level simulations of water and organic and biomolecular systems. *Proceedings of the National Academy of Sciences* **2005**, *102*, 6665–6670.

[2] Dodda, L. S.; De Vaca, I. C.; Tirado-Rives, J.; Jorgensen, W. L. LigParGen web server: An automatic OPLS-AA parameter generator for organic ligands. *Nucleic Acids Research* **2017**, *45*, W331–W336.

[3] Dodda, L. S.; Vilseck, J. Z.; Tirado-Rives, J.; Jorgensen, W. L. 1.14*CM1A-LBCC: Localized Bond-Charge Corrected CM1A Charges for Condensed-Phase Simulations. *Journal of Physical Chemistry B* **2017**, *121*, 3864–3870.

[4] Cygan, R. T.; Liang, J. J.; Kalinichev, A. G. Molecular models of hydroxide, oxyhydroxide, and clay phases and the development of a general force field. *Journal of Physical Chemistry B* **2004**, *108*, 1255–1266.

[5] Kerisit, S. Water structure at hematite-water interfaces. *Geochimica et Cosmochimica Acta* **2011**, *75*, 2043–2061.

[6] Boily, J. F. Water structure and hydrogen bonding at goethite/water interfaces: Implications for proton affinities. *Journal of Physical Chemistry C* **2012**, *116*, 4714–4724.

[7] Konuk, M.; Sellschopp, K.; Vonbun-Feldbauer, G. B.; Meißner, R. H. Modeling Charge Redistribution at Magnetite Interfaces in Empirical Force Fields. *Journal of Physical Chemistry C* **2021**, *125*, 4794–4805.

[8] Yeh, I. C.; Berkowitz, M. L. Ewald summation for systems with slab geometry. *Journal of Chemical Physics* **1999**, *111*, 3155–3162.